Optically and electrically co-controlled resistance switching in complex oxide heterostructures

Ming Zheng,[1,a)] Hao Ni,[1,2] Weiyi Huang,[1] Yaping Qi,[1] Jiali Zeng,[1] and Ju Gao[1,3,a)]
[1]*Department of Physics, The University of Hong Kong, Pokfulam Road, Hong Kong*
[2]*College of Science, China University of Petroleum, Qingdao 255680, China*
[3]*School of Mathematics and Physics, Suzhou University of Science and Technology, Suzhou 215009, China*

(Received 7 June 2017; accepted 8 October 2017; published online 23 October 2017)

The lattice degree of freedom has been utilized to pursue exotic functionalities in complex oxide heterostructures via various external stimuli, such as light, electric field, and magnetic field. Here, the epitaxial heterostructures composed of photostrictive $SrRuO_3$ thin films and ferroelectric $0.7Pb(Mg_{1/3}Nb_{2/3})O_3$-$0.3PbTiO_3$ single-crystal substrates are fabricated to investigate the light and electric field co-control of lattice order in resistance switching. The electric-field-induced strain-mediated electroresistance response can be effectively tuned by light illumination. This, together with the electric-field-tunable photoresistance effect, demonstrates strong correlation between the light and the electric field, which is essentially mediated by strain-driven lattice-orbital coupling. Our findings provide a platform for realizing multi-field tuning of the lattice degree of freedom and the resultant functionalities in complex oxide heterostructures. *Published by AIP Publishing.*
https://doi.org/10.1063/1.4986864

Strongly correlated complex oxides have attracted much attention for decades due to many intriguing physical phenomena, such as high temperature superconductivity, colossal magnetoresistance effect, electroresistance (ER) effect, magnetoelectric effect, photostrictive effect, and two-dimensional electron gas.[1–6] By controlling lattice, charge, spin, and orbital degrees of freedom in these oxides with various external stimuli, such as electric field, magnetic field, light, and strain, exotic functionalities are highly desired in the pursuit of low-power consumption, environmentally friendly, and multifunctional electronic devices. Of these degrees of freedom, the lattice degree of freedom is currently being extensively investigated since its energy scale is several orders of magnitude larger than others, offering a better design and control of new functionalities. As one of the most fascinating correlated materials, ferromagnetic metal $SrRuO_3$ (SRO) possesses attractive physical properties, such as exchange bias,[7] vertical hysteretic shift,[8] magnetocrystalline anisotropy,[9] and anomalous Hall effect,[10] for potential applications in spin valves and magnetic tunnel junctions.[11] The lattice degree of freedom in SRO films has been identified as the main factor to modify their physical properties by using external fields. For example, Herklotz *et al.*[12] and Zhou *et al.*[13] *in situ* imposed an in-plane compressive strain to SRO films epitaxially grown on the ferroelectric $Pb(Mg_{1/3}Nb_{2/3})O_3$-$PbTiO_3$ single crystals via the piezoelectric response and achieved lattice strain-mediated electric-field control of magnetic and electrical properties. In addition, SRO exhibits a striking dynamic visible-light-induced lattice variation, which arises from the non-equilibrium photo-population.[14–17] The light-induced photostrictive effect in SRO well exceeds that in multiferroic $BiFeO_3$[18] with a response time of 500 fs,[15] suggesting possible ultrafast photoelastic applications. This means that the light (or photos) can be introduced as an external control parameter to adjust the strain-coupled physical properties of SRO-based epitaxial heterostructures through the photostrictive effect. Actually, Schmising *et al.*[14] observed 2% and 100% changes of lattice tetragonality and polarization of a $PbZr_{0.2}Ti_{0.8}O_3$ sublayer in a $PbZr_{0.2}Ti_{0.8}O_3$/SRO superlattice system, respectively, via the optical-excited expansion of the SRO sublayer. Liu *et al.*[17] also reported light-induced magnetization changes in vertical heteroepitaxial $CoFe_2O_4$-SRO nanocomposites. However, while most of these studies have focused on *in situ* dynamic tuning of the lattice-coupled physical properties of SRO-based heterostructures using single electric field or light, rare attention has been paid to exploring multi-field combined control of the lattice degree of freedom and lattice-driven functionalities. There is no doubt that a systematic investigation of co-effects of the electric field and light on lattice distortion and physical properties of SRO-based heterostructures would help to shed further light on the strain effects and the coupling mechanism of the electric field and the light, as well as the design of energy-efficient multifunctional electronic and optical devices based on complex oxide heterostructures.

Motivated by this, we epitaxially grew photostrictive SRO thin films on ferroelectric $0.7Pb(Mg_{1/3}Nb_{2/3})O_3$-$0.3PbTiO_3$ (PMN-PT) single-crystal substrates and *in situ* manipulated the strain state of the SRO films through the electric-field-induced ferroelectric domain switching and the light-induced photostrictive effect, respectively. We paid particular attention to electrically and optically co-controlled strain-mediated resistance switching and the mutual interaction between the electric field and the light. Our study paves the way for performing electrically and optically co-coupled functionalities in heteroepitaxial complex oxide systems.

SRO thin films (~35 nm thick) were fabricated on ferroelectric (001)-oriented PMN-PT single-crystal substrates

a)Authors to whom correspondence should be addressed: zhengm@mail.ustc.edu.cn and jugao@hku.hk

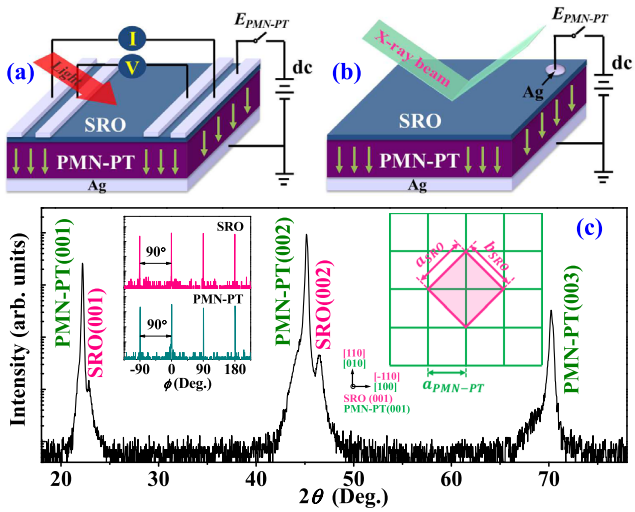

FIG. 1. Schematic of the experimental setups for *in situ* measurements of film resistance (a) and out-of-plane strain (b), respectively. (c) XRD θ-2θ scan of the SRO/PMN-PT structure. The left inset shows XRD ϕ scans taken on the SRO(101) and PMN-PT(101) diffraction peaks. The right inset shows a schematic of in-plane lattice arrangements for the orthorhombic SRO unit cell on the PMN-PT substrate.

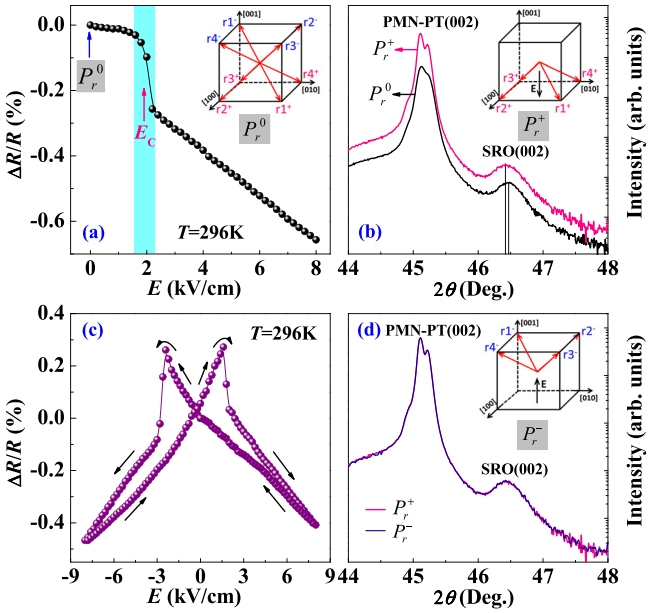

FIG. 2. (a) Electric-field-induced relative resistance change $\Delta R/R$ of the SRO film as a function of E applied across the PMN-PT at $T = 296$ K. (b) XRD θ-2θ scans for the PMN-PT(002) substrate and the SRO(002) film in the P_r^0 and P_r^+ states. (c) $\Delta R/R$ as a function of bipolar E. (d) XRD θ-2θ scans in the P_r^+ and P_r^- states. Insets: corresponding schematic of the polarization vectors in the rhombohedral phase in the P_r^0, P_r^+, and P_r^- states for the PMN-PT, respectively.

using the pulsed laser deposition technique. The deposition was conducted in pure oxygen of 150 mTorr at 680 °C followed by *in situ* annealing in pure oxygen of 1 atm for 30 min to reduce oxygen deficiencies. The crystal structure and the in-plane epitaxial relationship between the film and the substrate were examined by θ-2θ linear scan and ϕ-scan, respectively, using a high resolution Bruker D8 Discover X-ray diffractometer (XRD) equipped with Cu $K_{\alpha 1}$ radiation source ($\lambda = 1.5406$ Å). A Keithley 6487 voltage source was employed to supply an electric field applied across the PMN-PT substrate along the [001] crystal direction through the metallic SRO film and the thermal-evaporated bottom silver electrode. A semiconductor laser with a wavelength of 650 nm, a power density of 5 mW/cm^2, and a spot size of 50 μm^2 served as the light illumination source. Figures 1(a) and 1(b) display the schematic of the experimental setups for *in situ* measurements of resistance under the electric field and light illumination (using the standard four-probe method) and out-of-plane strains of the SRO film and the PMN-PT substrate (using *in situ* XRD θ-2θ scans), respectively.

Figure 1(c) shows the XRD θ-2θ scan pattern of the SRO film grown on the PMN-PT substrate. The SRO film has no impurity phases and is highly c-axis oriented. XRD ϕ-scans taken on the SRO (101) and PMN-PT (101) diffraction peaks yield two sets of fourfold symmetrical diffraction peaks recurring every 90° at the same azimuthal ϕ angle [see the left inset of Fig. 1(c)]. This result clearly describes the epitaxial relationship of $(001)_{SRO}||(001)_{PMN\text{-}PT}$ and $[100]_{SRO}||[100]_{PMN\text{-}PT}$ in the pseudocubic form, indicative of a cube-on-cube heteroepitaxy. A schematic diagram of the in-plane lattice arrangements for the orthorhombic SRO unit cell on the PMN-PT substrate is shown in the right inset of Fig. 1(c). The initial strain state of the SRO film can be determined by analyzing its main peak in the XRD scan curve. The estimated out-of-plane lattice constant c (~3.905 Å) is smaller than the bulk value (~3.93 Å),[11] suggesting that the SRO film suffers an out-of-plane compressive strain (−0.63%). Using Poisson's relation $\delta\varepsilon_{zz} = -2\nu/(1-\nu)\delta\varepsilon_{xx}$[19] and Poisson's ratio $\nu_{SRO} = 0.28$,[12] the in-plane tensile strain of the SRO film is calculated to be 0.81%, which is consistent with the smaller lattice constants of the SRO bulk than those of the PMN-PT substrate ($a \sim b \sim c \sim 4.02$ Å).

To explore the electric field effect on the SRO/PMN-PT heterostructure, we measured the relative change of resistance ($\Delta R/R$) of the SRO film as a function of the electric field applied across the PMN-PT substrate in Fig. 2(a). It was found that the film resistance exhibits a nonlinear abrupt drop near E_C (~2 kV/cm) of the PMN-PT substrate, implying the potential relation between the film resistance and the strain state of the substrate. *In situ* XRD measurements [see Fig. 2(b)] clearly show that after ferroelectric poling by applying a large positive electric field (e.g., $E = 8$ kV/cm), both the PMN-PT(002) and the SRO(002) diffraction peaks shift to lower 2θ angles, revealing an expansion along the out-of-plane direction accompanied by an effective in-plane contraction of both the PMN-PT and the SRO. The electric-field-induced out-of-plane tensile strain can be calculated to be 0.102% and 0.212% for the SRO film and the PMN-PT substrate, respectively. Using Poisson's relation $\delta\varepsilon_{zz} = -2\nu/(1-\nu)\delta\varepsilon_{xx}$, with $\nu_{SRO} = 0.28$ and $\nu_{PMN\text{-}PT} = 0.5$,[20] the induced in-plane compressive strain is estimated to be 0.079% and 0.106%, respectively. Thus, the effective strain transferring coefficient α is ~75% [$\alpha = \delta\varepsilon_{xx(SRO)}/\delta\varepsilon_{xx(PMN-PT)}$], hinting strong transferring of the induced in-plane strain from the PMN-PT substrate to the SRO film. It has been reported that the poling-induced remnant strain microscopically originates from the reorientation of ferroelectric domains in the PMN-PT single-crystal substrate.[21–24] As shown in the inset of Fig. 2(a), the eight

spontaneous polarization vectors of the rhombohedral PMN-PT crystal randomly point along the body diagonals of the pseudocubic cell in the initial or unpoled state (denoted by P_r^0), corresponding to four structural domains (r1, r2, r3, and r4). Upon applying a large poling electric field of $E = +8$ kV/cm, the 180° ferroelectric switching (e.g., from $r1^-$ to $r1^+$), 109° ferroelastic switching (e.g., from $r2^-/r4^-$ to $r1^+$), and 71° ferroelastic switching (e.g., from $r3^-$ to $r1^+$) take place, and, thus all the polarization vectors rotate downward, pointing along the [00-1] direction (denoted by the P_r^+ state) [see the inset of Fig. 2(b)]. As a result, an in-plane compressive strain can be produced in the PMN-PT substrate and transferred to the overlying SRO film after ferroelectric poling by the electric field, giving rise to the resistance change.

A more direct visualization of the strain effect is illustrated in Fig. 2(c), where $\Delta R/R$ was plotted against bipolar electric field E applied to the PMN-PT substrate. With the increase in the negative reverse E, a non-180° polarization reorientation occurs near the coercive field,[24] causing a large jump in resistance near E_C. The E_C value of the PMN-PT can be referred to our earlier work[25,26] and the reports by Jie *et al.*[27] and Chen *et al.*[28] With a further increase in the reverse E ($E > |-E_C|$), the polarization undergoes another non-180° reorientation,[24] accompanied by a sharp drop in the resistance. This two-stage polarization reorientation process leads to a 180° polarization switching for all domains, i.e., the polarization vectors point along the [001] direction (denoted by the P_r^- state) [see the inset of Fig. 2(d)]. Under such circumstance, no remnant strain was generated in the PMN-PT substrate from the P_r^+ to the P_r^- state, as reflected by the same peak position of the PMN-PT(002) reflections for these two polarization states in Fig. 2(d). Consequently, both the strain state and the resistance of the SRO film were not modulated after polarization reversal. Moreover, the $\Delta R/R$ versus E curve discloses a typical butterfly-like shape, resembling the butterfly-like strain curves of the PMN-PT.[25,26] This finding further confirms the strain-induced nature of the resistance evolution. Considering the infinitesimal screening length (1–2 Å) of the electron in SRO films,[29] it is reasonable to preclude the electric-field-induced electrostatic charge-mediated correlation mechanism in our 35 nm-thick SRO film.

Figure 3(a) shows the electroresistance (ER) effect of the SRO/PMN-PT heterostructures in the dark and under light illumination at room temperature. Here, ER is defined as $ER = [R(E) - R(0)]/R(0)$. Upon applying a positive electric field E to the positively poled (P_r^+) PMN-PT substrate, ER decreases linearly with increasing E from 0 to 8 kV/cm due to the converse-piezoelectric-effect-induced linear contraction of the in-plane lattice of the PMN-PT rather than domain switching mediation [see the lower left inset of Fig. 3(a)].[30] As depicted in Fig. 3(b), the out-of-plane strain $\delta\varepsilon_{zz(PMN-PT)}$ of the PMN-PT substrate indeed shows a linear response to the electric field, as calculated from *in situ* XRD measurements in the lower right inset of Fig. 3(b). Using Poisson's relation $\delta\varepsilon_{zz} = -2\nu/(1-\nu)\delta\varepsilon_{xx}$, the linear dependence of the ER of the film on the induced in-plane strain $\delta\varepsilon_{xx(PMN-PT)}$ of the substrate was obtained in the dark and under light illumination, respectively, as shown in the upper left inset of Fig. 3(b). This electroresistance-strain relationship demonstrates that the ER of the SRO film is proportional to the induced in-plane strain in the film. The presence of negative electroresistance of the film can be explained in terms of piezoelectric strain-driven lattice contraction-induced enhancement of the orbital overlap between the Ru 4*d* orbitals and O 2*p* orbitals by adjusting the octahedral rotations.[31,32] The enhanced orbital hybridization widens the one electron bandwidth and thus reduces the electron correlation effect, thereby decreasing the film resistance. It should be noted that the ER of the film is considerably reduced over the whole electric-field (or in-plane strain) range after light illumination. The relative change in ER, $\Delta ER/ER = (ER_{dark} - ER_{light})/ER_{dark}$, increases continuously with the increasing electric field and reaches a maximal value of 8.2% at $E = 8$ kV/cm, signaling the high sensitivity of the ER effect to the light at high electric fields. The significant impact of light on electroresistance is also evident in the upper right inset of Fig. 3(a), where ER was plotted against time in the dark and under light illumination when the electric field of $E = 8$ kV/cm was turned on and off. Such an optically controlled electroresistance

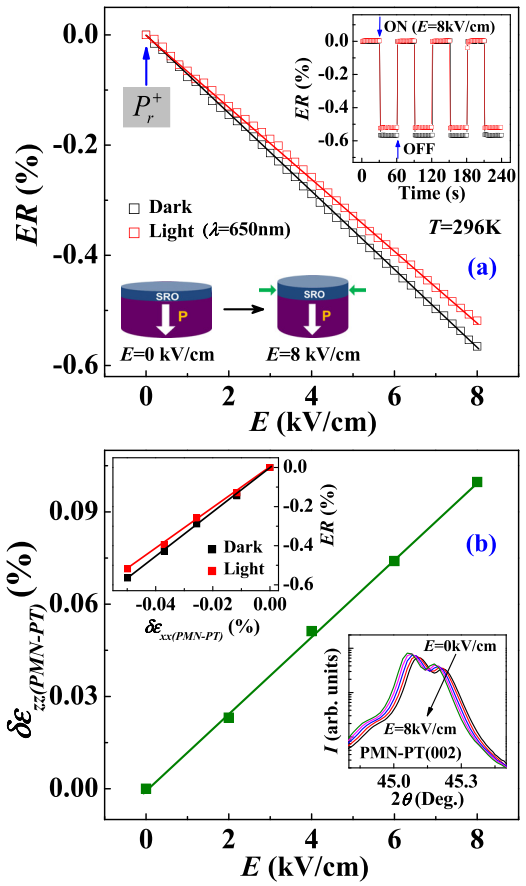

FIG. 3. (a) The electroresistance ER of the SRO film as a function of positive E applied to the positively poled PMN-PT substrate in the dark and under light illumination ($\lambda = 650$ nm) at $T = 296$ K. The upper right inset shows the ER curves of the SRO film in the dark and under light illumination when the electric field of $E = 8$ kV/cm was turned on and off. The lower left inset shows schematic diagrams for the converse piezoelectric effect. (b) Electric-field-induced out-of-plane strain $\delta\varepsilon_{zz(PMN-PT)}$ of the PMN-PT substrate as a function of E. The upper left inset shows the ER of the SRO film as a function of in-plane strain $\delta\varepsilon_{xx(PMN-PT)}$ of the PMN-PT substrate. The lower right inset shows *in situ* XRD θ-2θ scans for the PMN-PT(002) under different electric fields.

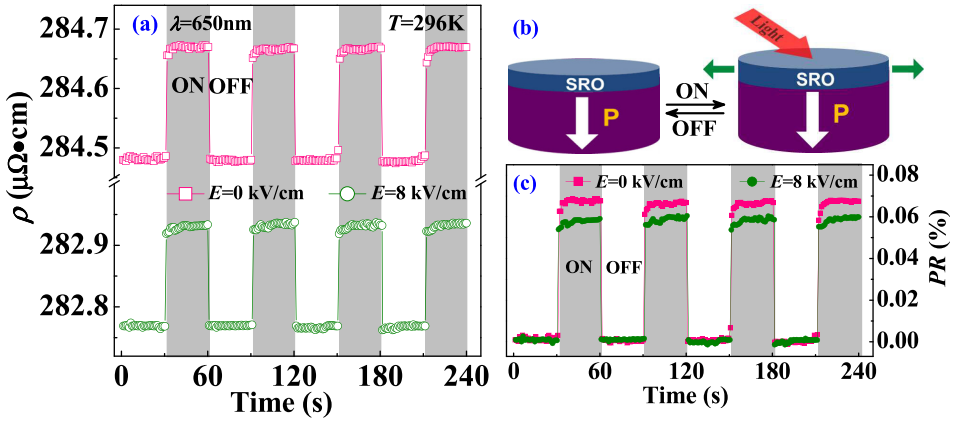

FIG. 4. (a) The resistance switching of the SRO film in the dark and under light illumination ($\lambda = 650$ nm) with and without the application of $E = 8$ kV/cm to the PMN-PT at $T = 296$ K. (b) Schematic diagrams for the photostrictive effect. (c) The photoresistance curves of the SRO film when the light was turned on and off with and without the application of $E = 8$ kV/cm to the PMN-PT at $T = 296$ K, respectively.

response can be ascribed to the optical-excited lattice expansion that reduces the orbital hybridization of the SRO films, thus suppressing the converse piezoelectric effect of the SRO/PMN-PT structure. This finding demonstrates the effectiveness of light tunability of the lattice degree of freedom.

The mutual interaction between the electric field and the light is manifested not only by the light-tunable electroresistance effect but also by the electric-field-tunable photoresistance effect. The latter effect is shown in Fig. 4(a), where the photo-induced variation of resistance (i.e., photoresistance) of the SRO film was recorded by turning the light on and off with and without the application of $E = 8$ kV/cm to the PMN-PT at room temperature. Here, the photoresistance is defined as $PR = (R_{light} - R_{dark})/R_{dark}$. For $E = 0$ kV/cm, a stable and distinct light-induced enhancement of resistance (i.e., positive photoresistance of 0.066%) was observed, which is superior to earlier reports on SRO films.[33] This finding can be attributed to the visible-light-induced lattice expansion [see Fig. 4(b)] and the resulting decrease in the orbital overlap of the SRO films.[14–17] Under light illumination, optical absorption initially heats the electrons, and these give up their energy to phonons to produce the strain through direct electron-phonon interactions.[15] The light-induced lattice expansion can reduce orbital hybridization between the Ru 4d orbitals and O 2p orbitals, which lowers the one electron bandwidth and enhances the electron correlation effect, leading to the increase in the resistance. It has been demonstrated that photo-excitation induces transient strain in $SrRuO_3$ on a timescale of 500 fs.[15] In Fig. 4(a), the resistance was recorded by turning the light on and off with an interval of 30 s. The system has returned to its equilibrium state during the measurement period after turning the light on and off. In addition, SRO is known to have a very large electron-electron scattering rate and fast electron-phonon relaxation time on the order of a few hundred femtoseconds, which is much faster than any diffusion processes of electrons and phonons.[34] When considering the structural dynamics in thin SRO films on the timescale of a few tens of seconds, we can thus disregard the heat diffusion. Even if light illumination creates a little heat, the heat can also be dissipated into the substrate mounted on the Cu plate, and the system returns to its equilibrium state after about 10 ns. Therefore, the heating effect can be ignored. Upon applying an electric field of $E = 8$ kV/cm, the film resistance was reduced dramatically, as discussed earlier. Meanwhile, the film also displays a noticeable photostrictive effect on the resistance switching during light illumination. Obviously, the photoresistance is suppressed by ~11.4% as the electric field is increased from $E = 0$ to 8 kV/cm, as illustrated in Fig. 4(c). The electrically tunable photoresistance effect stems from the piezoelectric strain-induced enhancement of orbital hybridization, which suppresses the photostrictive effect of SRO/PMN-PT structure. These data together establish that the electric field strongly correlates with the light, which is deeply mediated by strain-driven lattice-orbital coupling.

In summary, we reported the light and electric field co-control of lattice-coupled functionalities using the well-designed SRO/PMN-PT epitaxial heterostructures. The electric-field-induced converse piezoelectric effect of the PMN-PT substrate enables the in-plane lattice contraction of the SRO film, which, in turn, moderately reduces the film resistance. The electroresistance response can be tuned by 8.2% under light illumination. In contrast, the visible-light-induced lattice expansion leads to a remarkable increase in the film resistance. Such a photoresistance effect was found to be electrically tunable. These results reveal that the light and the electric field strongly couple with each other, which can be reasonably interpreted by strain/lattice distortion modulation of orbital hybridization between the Ru 4*d* orbitals and O 2*p* orbitals. This work opens a unique gate to explore multi-field tuning of the lattice degree of freedom and lattice-driven functionalities and design low-power consumption multifunctional optical and electronic devices based on complex oxide systems using strain engineering.

This work was supported by the National Key Project for Basic Research (Grant No. 2014CB921002), the National Natural Science Foundation of China (Grant Nos. 11374225, 11574227, and 11504432), the Shandong Provincial Natural Science Foundation, China (Grant No. BS2015DX002), and the Research Grant Council of Hong Kong (Project No. HKU 702112P). This work is also supported by the PAPD, the Key Engineering Laboratory of Jiangsu DRC, Suzhou Key Laboratory for Low Dimensional Optoelectronic Materials and Devices (SZS201611), and USTS Cooperative Innovation Center.

[1]P. A. Lee, N. Nagaosa, and X.-G. Wen, Rev. Mod. Phys. **78**, 17 (2006).
[2]M. Uehara, S. Mori, C. H. Chen, and S.-W. Cheong, Nature **399**, 560 (1999).

[3]V. Garcia and M. Bibes, Nat. Commun. **5**, 4289 (2014).
[4]P. Yu, Y.-H. Chu, and R. Ramesh, Mater. Today **15**, 320 (2012).
[5]P. Poosanaas, A. Dogan, S. Thakoor, and K. Uchino, J. Appl. Phys. **84**, 1508 (1998).
[6]A. Ohtomo and H. Y. Hwang, Nature **427**, 423 (2004).
[7]C. Sow, A. K. Pramanik, and P. S. Anil Kumar, J. Appl. Phys. **116**, 194310 (2014).
[8]L. Pi, S. X. Zhang, S. Tan, and Y. H. Zhang, Appl. Phys. Lett. **88**, 102502 (2006).
[9]X. W. Wang, Y. Q. Zhang, H. Meng, Z. J. Wang, D. Li, and Z. D. Zhang, J. Appl. Phys. **109**, 07D707 (2011).
[10]Z. Fang, N. Nagaosa, K. S. Takahashi, A. Asamitsu, R. Mathieu, T. Ogasawara, H. Yamada, M. Kawasaki, Y. Tokura, and K. Terakura, Science **302**, 92 (2003).
[11]G. Koster, L. Klein, W. Siemons, G. Rijnders, J. S. Dodge, C. B. Eom, D. H. A. Blank, and M. R. Beasley, Rev. Mod. Phys. **84**, 253 (2012).
[12]A. Herklotz, M. Kataja, K. Nenkov, M. D. Biegalski, H.-M. Christen, C. Deneke, L. Schultz, and K. Dörr, Phys. Rev. B **88**, 144412 (2013).
[13]W. P. Zhou, Q. Li, Y. Q. Xiong, Q. M. Zhang, D. H. Wang, Q. Q. Cao, L. Y. Lv, and Y. W. Du, Sci. Rep. **4**, 6991 (2014).
[14]C. v. K. Schmising, M. Bargheer, M. Kiel, N. Zhavoronkov, M. Woerner, T. Elsaesser, I. Vrejoiu, D. Hesse, and M. Alexe, Phys. Rev. Lett. **98**, 257601 (2007).
[15]C. v. Korff Schmising, A. Harpoeth, N. Zhavoronkov, Z. Ansari, C. Aku-Leh, M. Woerner, T. Elsaesser, M. Bargheer, M. Schmidbauer, I. Vrejoiu, D. Hesse, and M. Alexe, Phys. Rev. B **78**, 060404 (2008).
[16]A. Bojahr, D. Schick, L. Maerten, M. Herzog, I. Vrejoiu, C. v. Korff Schmising, C. Milne, S. L. Johnson, and M. Bargheer, Phys. Rev. B **85**, 224302 (2012).
[17]H.-J. Liu, L.-Y. Chen, Q. He, C.-W. Liang, Y.-Z. Chen, Y.-S. Chien, Y.-H. Hsieh, S.-J. Lin, E. Arenholz, C.-W. Luo, Y.-L. Chueh, Y.-C. Chen, and Y.-H. Chu, ACS Nano **6**, 6952 (2012).
[18]B. Kundys, M. Viret, D. Colson, and D. O. Kundys, Nat. Mater. **9**, 803 (2010).
[19]S. P. Timoshenko and J. N. Goodier, *Theory of Elasticity* (McGraw-Hill, New York, 1987), Chap. 2.
[20]C. Thiele, K. Dörr, S. Fähler, L. Schultz, D. C. Meyer, A. A. Levin, and P. Paufler, Appl. Phys. Lett. **87**, 262502 (2005).
[21]S. Zhang, Y. G. Zhao, P. S. Li, J. J. Yang, S. Rizwan, J. X. Zhang, J. Seidel, T. L. Qu, Y. J. Yang, Z. L. Luo *et al.*, Phys. Rev. Lett. **108**, 137203 (2012).
[22]M. Liu, B. M. Howe, L. Grazulis, K. Mahalingam, T. X. Nan, N. X. Sun, and G. J. Brown, Adv. Mater. **25**, 4886 (2013).
[23]T. X. Nan, M. Liu, W. Ren, Z. G. Ye, and N. X. Sun, Sci. Rep. **4**, 5931 (2014).
[24]T. Wu, A. Bur, P. Zhao, K. P. Mohanchandra, K. Wong, K. L. Wang, C. S. Lynch, and G. P. Carman, Appl. Phys. Lett. **98**, 012504 (2011).
[25]M. Zheng, X. Y. Li, M. M. Yang, Q. X. Zhu, Y. Wang, X. M. Li, X. Shi, H. L. W. Chan, X. G. Li, H. S. Luo, and R. K. Zheng, Appl. Phys. Lett. **103**, 263507 (2013).
[26]M. Zheng and R. K. Zheng, Phys. Rev. Appl. **5**, 044002 (2016).
[27]W. Jie, Y. Y. Hui, N. Y. Chan, Y. Zhang, S. P. Lau, and J. Hao, J. Phys. Chem. C **117**, 13747 (2013).
[28]Y. Chen, Y. Zhang, D. Karnaushenko, L. Chen, J. H. Hao, F. Ding, and O. G. Schmidt, Adv. Mater. **29**, 1605165 (2017).
[29]C. H. Ahn, R. H. Hammond, T. H. Geballe, M. R. Beasley, J.-M. Triscone, M. Decroux, Ø. Fischer, L. Antognazza, and K. Char, Appl. Phys. Lett. **70**, 206 (1997).
[30]R. K. Zheng, Y. Jiang, Y. Wang, H. L. W. Chan, C. L. Choy, and H. S. Luo, Phys. Rev. B **79**, 174420 (2009).
[31]A. Vailionis, W. Siemons, and G. Koster, Appl. Phys. Lett. **93**, 051909 (2008).
[32]W. L. Lu, K. H. He, W. D. Song, C. J. Sun, G. M. Chow, and J. S. Chen, J. Appl. Phys. **113**, 17E125 (2013).
[33]H. J. Liu, T. C. Wei, Y. M. Zhu, R. R. Liu, W. Y. Tzeng, C. Y. Tsai, Q. Zhan, C. W. Luo, P. Yu, J. H. He, Y. H. Chu, and Q. He, Adv. Funct. Mater. **26**, 729 (2016).
[34]D. Schick, M. Herzog, A. Bojahr, W. Leitenberger, A. Hertwig, R. Shayduk, and M. Bargheer, Struct. Dyn. **1**, 064501 (2014).